Progress In Electromagnetics Research Letters, Vol. 97, 51–59, 2021

Compact Quarter Mode and Eighth Mode Substrate Integrated Waveguide Bandpass Filters with Frequency-Dependent Coupling

Zhiwei Shi, Guohui Li*, Yulu Song, and Binbin Cheng

Abstract—This paper presents two size-miniaturized quarter mode (QM) and eighth mode (EM) substrate integrated waveguide (SIW) bandpass filters (BPFs), which are embedded with a novel frequency-dependent coupling (FDC) structure. The proposed FDC is implemented as a composition of balanced folding lines and inductive iris. One additional transmission zero (TZ) introduced by FDC between two cavities leads to higher frequency selectivity and better out-of-band rejection. Higher order modes suppression appears by combining the loaded open stubs on feeder lines with FDC technique, achieving a wide stopband. Meanwhile, the circuit dimension is further reduced by symmetrically cutting SIW. To validate the novel approach, the frequency-dependent coupling matrix (CM) is implemented to determine characteristics of the proposed structure in theory. QM- and EM-SIW BPFs loaded with FDC have been designed, fabricated, and measured. Experimental results illustrate the characteristics of miniaturization and good performance. All results are in good agreement.

1. INTRODUCTION

With increasing demands for modern communication systems, miniaturization and high selectivity microwave bandpass filters (BPFs) have become urgently demanded. Substrate integrated waveguide (SIW) circuits [1–9] have attracted wide attention due to various advantages and characteristics, such as easy fabrication, high power handling capability, low insertion loss (IL), and easy integration with other circuits. However, conventional SIW filters still have relatively large circuit sizes. Recently, half-mode (HM) [1], quarter-mode (QM) [2], and eighth-mode (EM) [3] SIW have been proposed, which decrease the dimension to 50%, 25%, and 12.5%, respectively, while maintaining the performance unchanged. To obtain high selectivity, FDC techniques [4–13] introduce additional finite transmission zeros without changing the topology and filter size. For SIW, due to its excellent coplanar properties, both constant and frequency-dependent couplings can be performed on it with positive effects. From the multimode property of microwave resonant cavities, undesired parasitic coupling may occur, which degrades the stopband performance of the SIW filter severely, and ineffective resonance occurs near the passband [13]. Due to the harmonic effects caused by the FDC structure in EMSIW, coupling occurs among TE_{102}, TE_{201}, and TE_{202} higher order modes [14]. A pair of open circuit stubs, loading on the feeder side, are used to suppress spurious higher-order modes [15].

In this paper, a coupling matrix (CM) synthesis procedure [9–12] is implemented to design second order filters: QMSIW and EMSIW. The detailed parameters of discontinuous structures containing FDC [4–8] are theoretically synthesized and simulated. As expected, one transmission zero is generated at the frequency point, where electric coupling cancels out with magnetic coupling for the designed BPFs by frequency dependent coupling between cavities. Sharp passband skirts for two filters are up to 72 dB and 56 dB, respectively. Slicing technology makes it possible to achieve miniaturization on a single layer substrate without degrading the performance of the filters, while the circuit sizes are reduced up

Received 22 January 2021, Accepted 17 March 2021, Scheduled 29 March 2021
* Corresponding author: Guohui Li (ghlee@shu.edu.cn).
The authors are with the Key Laboratory of Specialty Fiber Optics and Optical Access Network, Shanghai University, China.

to 75% and further to 87.5%. In the meantime, it provides high-order mode (TE_{102}, TE_{201}, and TE_{202}) suppression based on FDC technique and open circuit stub, which is considered as a band-stop filter at the points of higher mode resonance. The almost 20 dB stopband suppression is achieved over 8.09 GHz. The designed procedure, simulated and measured results are discussed in the following sections.

2. ANALYSIS OF FDC STRUCTURE

The proposed FDC structure is composed of two balanced folding lines which are etched on the top layer of the circuit, as shown in Fig. 1. It is placed in the middle of the inductive iris between two cavities. Two open ends with the maximum electric fringe field density produce electric coupling, while the inductive iris mainly dominates the magnetic coupling. Hence, mixed coupling occurs. When the SIW resonant cavity operates TE_{101} mode, the field distribution in the resonant cavity is symmetric. Based on this property, the SIW resonant cavity is cut in the way shown in Fig. 2, and filter design can thus be miniaturized by cutting the SIW cavity. All parameters are simulated and designed on HFSS using Rogers RT/Duroid 5880 dielectric substrate with $\varepsilon_r = 0.2$, $h = 0.508$ mm.

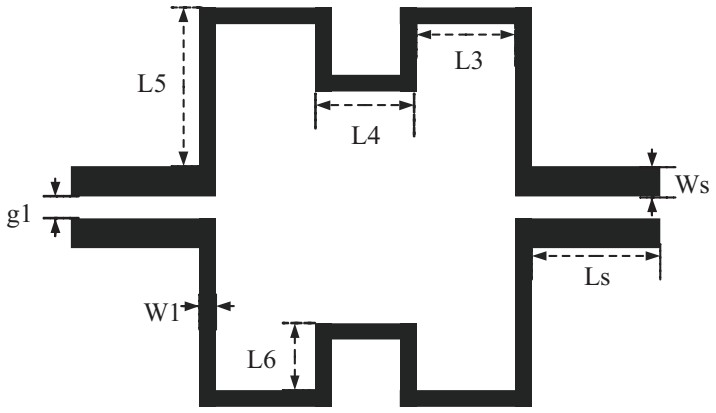

Figure 1. FDC structure between two cavities.

Based on FDC structure, two SIW bandpass filters are designed, as shown in Fig. 3. To explain the design more precisely, the normalized impedance characteristics K/Z_0 and coupling coefficient k_{ij} are derived with respect to different parameters, as illustrated in Fig. 4–Fig. 7. The normalized impedance inverter K/Z_0 from Eq. (1) will vanish at a particular frequency point to assess the position of TZ. By adjusting the length of L_S or the width of the inductive iris g_0, the electrical or magnetic coupling changes accordingly. It is apparent that mixed coupling can be dominated as positive or negative with different physical dimensions. As shown in Fig. 4 and Fig. 5, the position of TZ shifts towards lower frequency with L_S and g_0 increasing. When W_S is increased, the slope of the curve decreases, and the position of TZ shifts towards higher frequency. From Eq. (2), the coupling coefficient $k_{i,j}$ against relevant variables at the central frequency can be extracted as shown in Fig. 6 and Fig. 7. It is clear that as the ratio of L_5 and L_6 varies, the coupling coefficient changes slowly while keeping the slope almost invariant. However, the detailed analysis of above parameters cannot be applied to determine the accurate dimensions, L_S, W_S and g_0, and some further adjustments may still be required.

$$jK/Z_0 = Z_{21}/Z_0 \tag{1}$$

$$k_{i,j} = \pm\frac{f_1^2 - f_2^2}{f_1^2 + f_2^2} \tag{2}$$

where K is the impedance inverter; Z_0 is the characteristic impedance of SIW; Z_{21} is the open circuit transfer impedance; f_1 and f_2 are two split resonance frequencies; $k_{i,j}$ is the coupling coefficient.

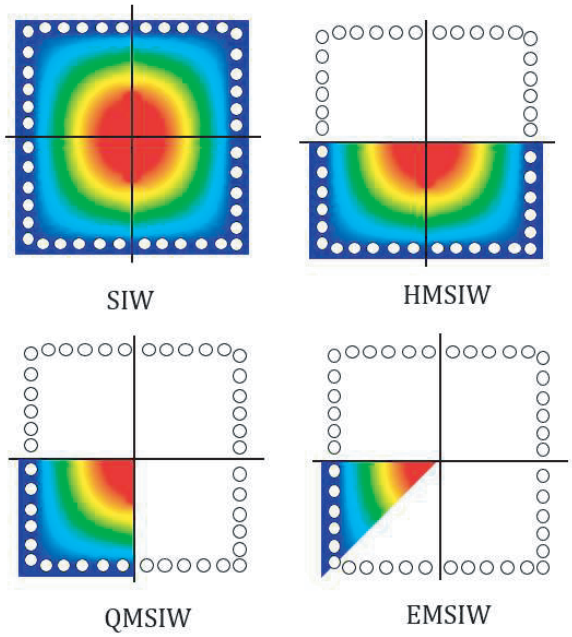

Figure 2. Electric field distributions of SIW, HMSIW, QMSIW and EMSIW.

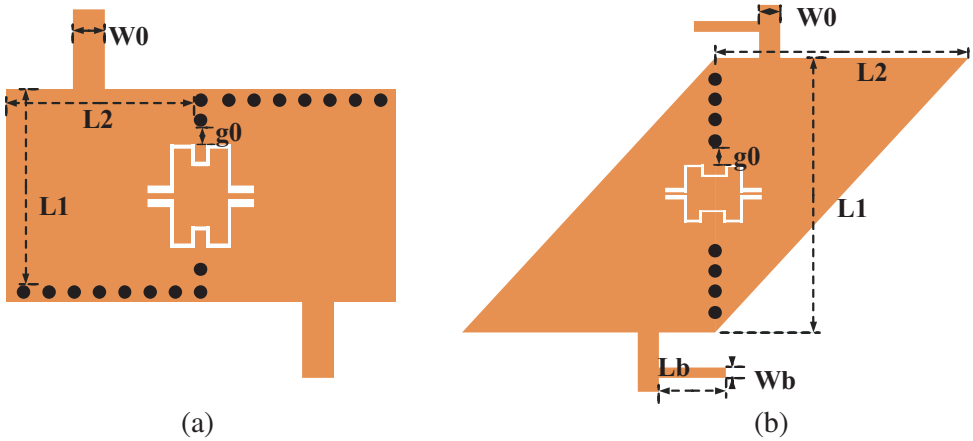

Figure 3. Layout of proposed SIW filters. (a) Filter IQMSIW. (b) Filter IIEMSIW.

3. FILTERS DESIGN AND EXPERIMENTAL VALIDATION

To demonstrate the performance of the proposed FDC structure, QM and EM cavities are used to design SIW BPFs. Coupling matrix (CM) synthesis procedure in [4–12] serves as a theoretical guide to the filters design, where TZ is generated at upper stopband. Besides, broad stopband technique in [13–15] has been implemented to suppress higher parasitic modes for filter II (QMSIW). It is then noticed that these two methods offer higher selectivity.

3.1. Filter I (QMSIW)

For demonstration, filter I with central frequency (CF) of 8 GHz and bandwidth (BW) of 1.8 GHz is constituted of two quarter mode cavities. Fig. 3(a) shows its top view configuration, and the FDC structure etched between two cavities produces one finite TZ on the upper stopband at 12 GHz.

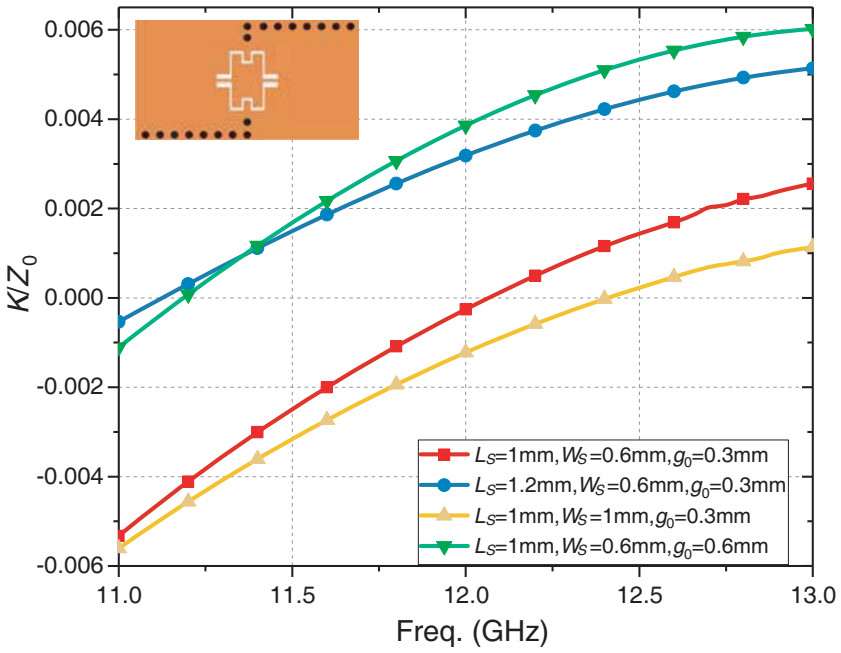

Figure 4. Normalized impedance characteristics (K/Z_0) with different parameters for Filter I.

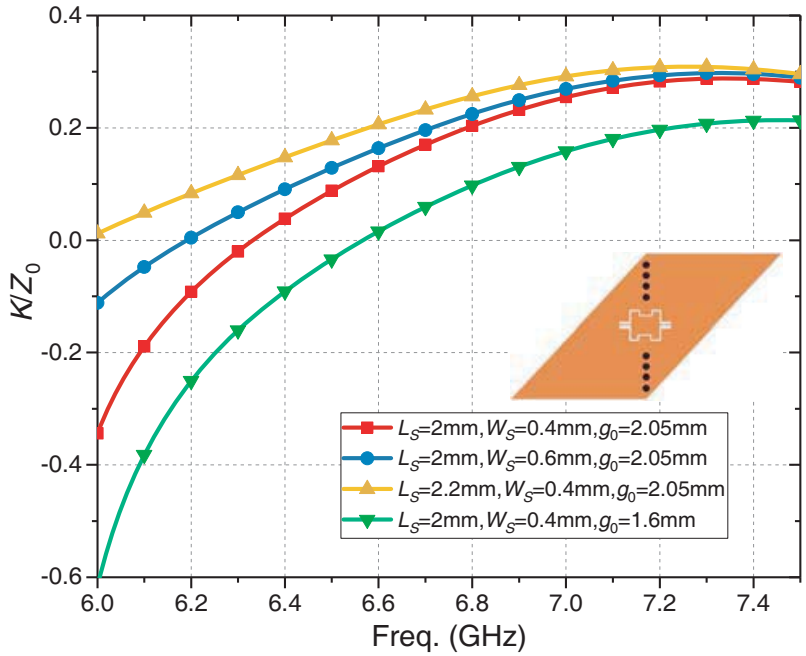

Figure 5. Normalized impedance characteristics (K/Z_0) with different parameters for Filter II.

The CM in Eq. (3) is obtained according to the steps of synthesis and optimization in [9–12], where ω denotes the normalized angular frequency. All parameters have been determined and optimized from Fig. 4 and Fig. 6. The final dimensions are as follows: $L_S = 1$, $W_S = 0.3$, $L_1 = 9.1$, $L_2 = 7.61$, $L_3 = 0.8$, $L_4 = 0.8$, $L_5 = 2.5$, $L_6 = 0.4$, $W_0 = 1.52$, $W_1 = 0.2$, $g_0 = 0.3$, $g_1 = 0.2$ (unit: mm). Comparison between the measured and simulated scattering parameters of the fabricated Filter I is presented in Fig. 8. Filter I has a compact size of $19.82 \times 20.1\,\text{mm}^2$ ($0.43 \times 0.44\ \lambda_g^2$), and relevant schematic image of circuit is also

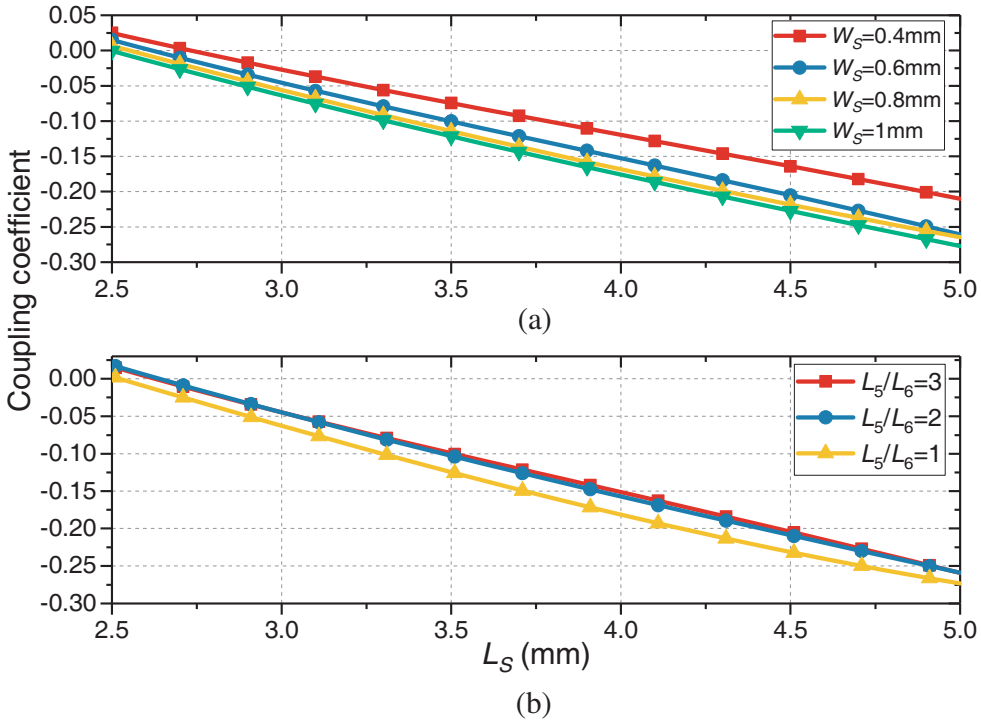

Figure 6. Variation of coupling coefficients with L_S for relevant variables. (a) Parameter W_S. (b) Parameter L_5/L_6. Filter I.

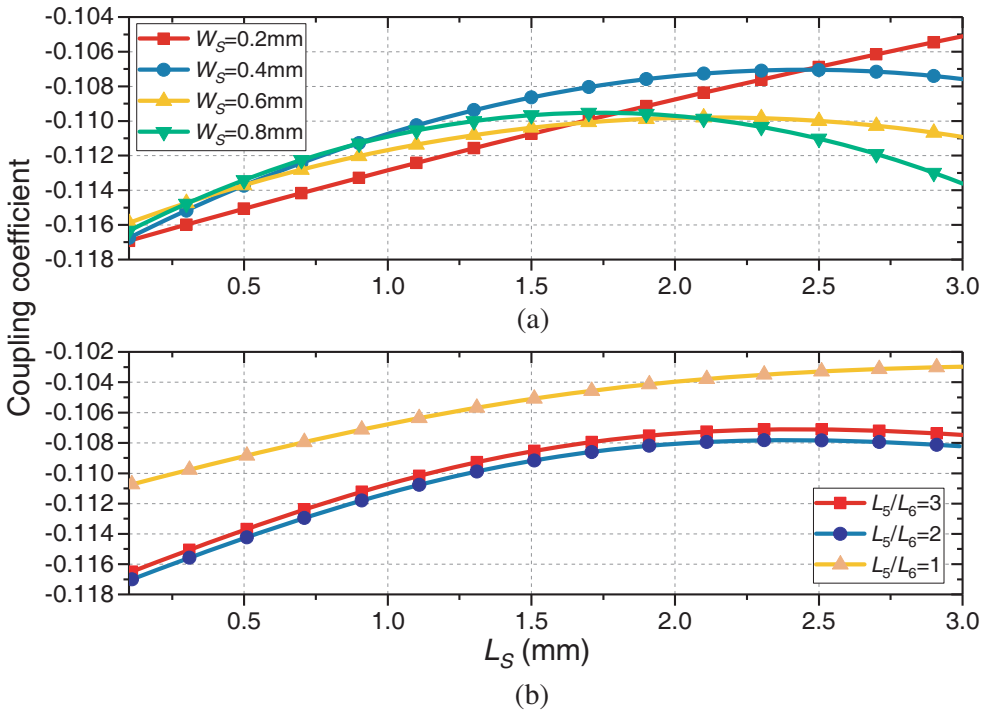

Figure 7. Variation of coupling coefficients with L_S for relevant variables. (a) Parameter W_S. (b) Parameter L_5/L_6. Filter II.

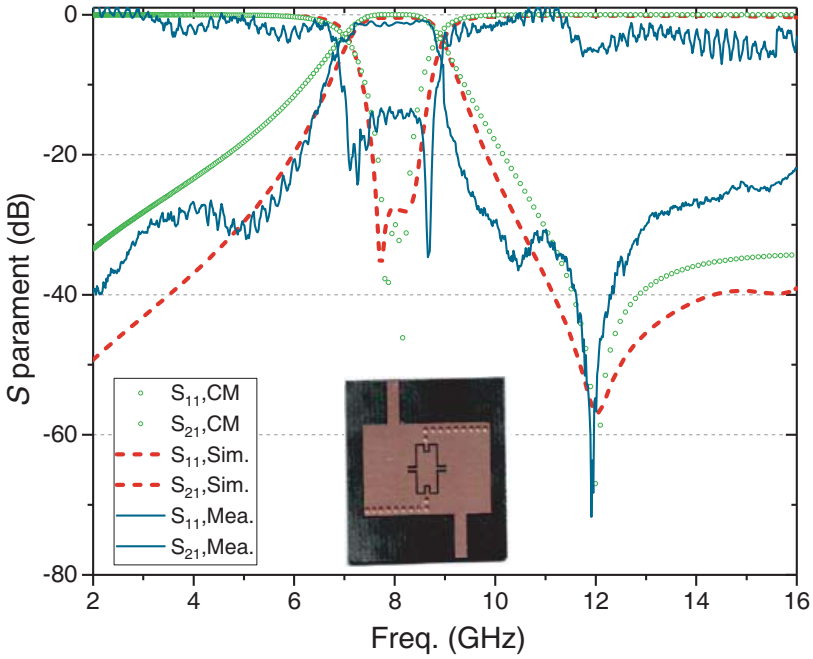

Figure 8. S parameter comparison of CM, simulation and measurement for Filter I.

inserted in Fig. 8. The measured insertion loss (IL) is, in the worst case, equal to 1.59-dB, with CF and BW of 7.95 GHz and 1.7 GHz, respectively. The filter in-band return loss (RL) is below 13.18 dB which is mainly caused by inaccurate fabrication, and extra loss comes from SMA connectors. As can be seen, the measured TZ at 11.91 GHz providing a higher selectivity is nearly as designed.

$$\begin{bmatrix} 0 & -1.6382 & 0 & 0 \\ -1.6382 & -0.5794 & -2.8316+0.1987\omega & 0 \\ 0 & -2.8316+0.1987\omega & -0.5794 & 1.6382 \\ 0 & 0 & 1.6382 & 0 \end{bmatrix} \tag{3}$$

3.2. Filter II (EMSIW)

As another example, a second-order at the center frequency of 3.4 GHz multi-mode filter with 500 MHz bandwidth by bisecting the QMSIW cavity along magnetic walls is designed and fabricated based on the previous methods, as shown in Fig. 3(b). One finite TZ of 6.4 GHz is located on the upper stopband. The introduction of electrical and magnetic coupling can counteract one of the TE_{102} (TE_{102}) or TE_{202} modes [13]. However, it still cannot suppress these two higher-order modes simultaneously, as illustrated in Fig. 8. To enhance the selectivity and out-of-band rejection characteristics, a pair of open circuit stubs which can be regarded as quarter-wavelength resonators are incorporated into the feed structure to suppress the effects of higher-order modes. As can be seen from Fig. 9, the loading stubs effectively suppress higher-modes, bringing S_{21} down to around -40 dB. The TE mode resonant frequency is determined by:

$$f_{TE_{m0n}} = \frac{c}{2\sqrt{\mu_r \varepsilon_r}} \sqrt{\left(\frac{m}{a_{eff}}\right)^2 + \left(\frac{n}{l_{eff}}\right)^2} \tag{4}$$

$$a_{eff} = a - \frac{d^2}{0.95p} \tag{5}$$

$$l_{eff} = l - \frac{d^2}{0.95p} \tag{6}$$

where c is the velocity of light in vacuum; ε_r and μ_r are the relative permittivity and permeability of the substrate; m and n represent the mode in dices of x- and z-axes; a and l represent the width and length of the cavity with the same length equal to 123.8 mm. The metallized via holes were made with a diameter of $d = 0.6$ mm and a center-to-center pitch of $p = 0.95$ mm. From Eq. (4), the calculated resonant frequencies are 6.079 GHz (TE_{102} or TE_{201}), 7.689 GHz (TE_{202}), and 3.845 GHz (TE_{101}), which are consistent with the simulation results shown in Fig. 9. The final dimensions were adjusted to match

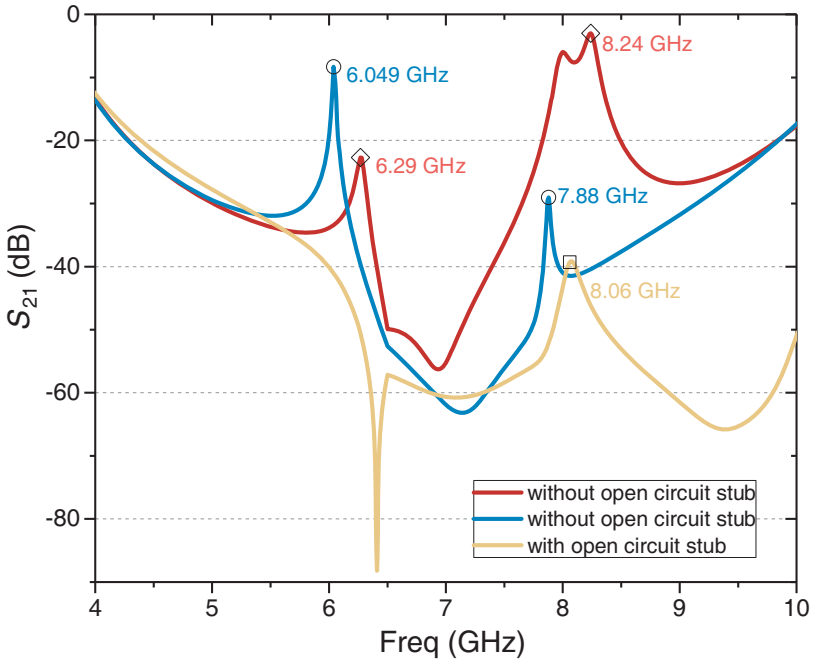

Figure 9. Comparison between filter II with/without open circuit stub.

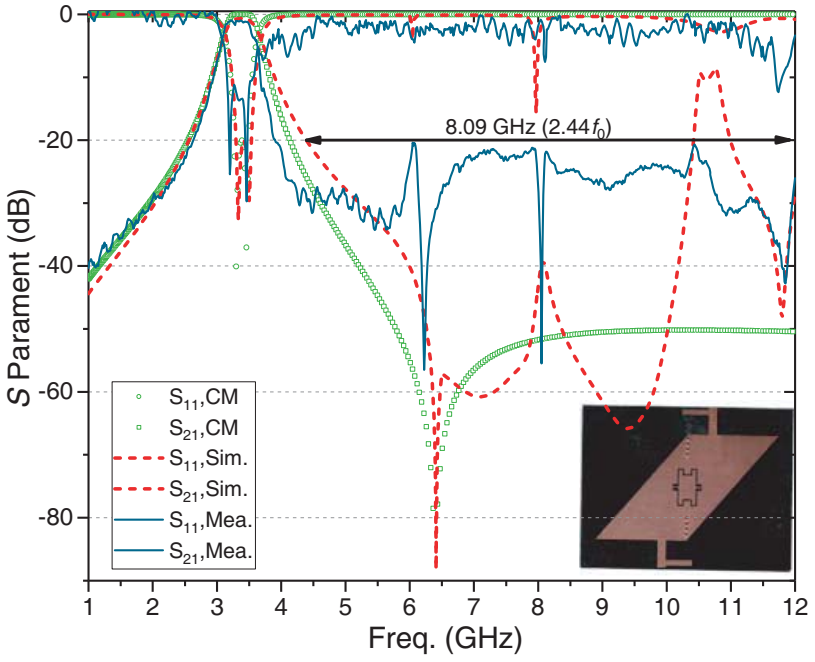

Figure 10. S parameter comparison of CM, simulation and measurement for Filter II.

the characteristic obtained from the coupling matrix in Eq. (7) as follows: $L_S = 1$, $W_S = 0.4$, $L_1 = 19$, $L_2 = 18.9$, $L_3 = 0.85$, $L_4 = 1.9$, $L_5 = 2.8$, $L_6 = 1$, $W_0 = 1.8$, $W_1 = 0.2$, $g_0 = 2.05$, $g_1 = 0.3$, $L_b = 5.5$, $W_b = 1$ (unit: mm). The final S parameter comparisons of CM, simulation, and measurement are depicted in Fig. 10, and the whole filter size is $43.8 \times 29\,\text{mm}^2$ ($0.23 \times 0.15\lambda_g^2$). The measured IL equals 1.69-dB in the worst case with CF and BW of 3.31 GHz and 440 MHz, respectively. The RL is 11.18-dB larger than the simulated one at the upper stopband. It is interesting to observe that the location of the measured transmission zero at 6.23 GHz is completely coincident with that of the simulated one. The stopband is significantly extended to 8.09 GHz ($2.44f_0$) with a suppression level larger than 20 dB, which indicates higher selectivity.

$$\begin{bmatrix} 0 & -1.2215 & 0 & 0 \\ -1.2215 & -0.1492 & -1.6568+0.0826\omega & 0 \\ 0 & -1.6568+0.0826\omega & -0.1492 & 1.2215 \\ 0 & 0 & 1.2215 & 0 \end{bmatrix} \tag{7}$$

4. CONCLUSION

In this paper, a novel structure constituting of balanced folding lines and inductive iris has been presented to realize a mixed electric and magnetic coupling. An additional controllable TZ appears, thereby resulting in a sharp passband skirt. Representative design examples of QMSIW and EMSIW filters are designed, fabricated, and measured to illustrate the characteristics of FDC structure. In the meantime, a pair of stubs were loaded on the EMSIW feed lines to suppress higher-order modes, contributing to a wide stopband. Both filters have the advantages of compact circuit size and high selectivity.

REFERENCES

1. Shen, W., "Extended-doublet half-mode substrate integrated waveguide bandpass filter with wide stopband," *IEEE Microw. Wireless Compon. Lett.*, Vol. 28, No. 4, 305–307, Apr. 2018.
2. Li, P., H. Chu, and R.-S. Chen, "Design of compact bandpass filters using quarter-mode and eighth-mode SIW cavities," *IEEE Trans. Compon. Packaging Manuf. Technol.*, Vol. 7, No. 6, 956–963, Jun. 2017.
3. Li, L., Z. Wu, K. Yang, X. Lai, and Z. Lei, "A novel miniature single-layer eighth-mode SIW filter with improved out-of-band rejection," *IEEE Microw. Wireless Compon. Lett.*, Vol. 28, No. 5, 407–409, May 2018.
4. Szydlowski, L., A. Jedrzejewski, and M. Mrozowski, "A trisection filter design with negative slope of frequency-dependent cross coupling implemented in substrate integrated waveguide (SIW)," *IEEE Microw. Wireless Compon. Lett.*, Vol. 23, No. 9, 456–458, Sep. 2013.
5. Szydlowski, L., N. Leszczynska, and M. Mrozowski, "A linear phase filter in quadruplet topology with frequency-dependent couplings," *IEEE Microw. Wireless Compon. Lett.*, Vol. 24, No. 1, 32–34, Jan. 2014.
6. Jedrzejewski, A., L. Szydlowski, and M. Mrozowski, "Miniaturized bandpass substrate integrated waveguide filter with frequency dependent coupling realized using a symmetric GCPW discontinuity," *Microw. Opt. Technol. Lett.*, Vol. 57, No. 8, 1818–1821, Aug. 2015.
7. Li, X., C. You, H. Yu, and Z. He, "Substrate integrated folded waveguide controllable mixed electric and magnetic coupling structure and its application to millimetre-wave pseudo-elliptic filters," *Int. J. RF Microw. Comput. Aided Eng.*, Vol. 27, e21074, 2017.
8. Liu, Q., D. Zhou, D. Zhang, and D. Lv, "A novel frequency-dependent coupling with flexibly controllable slope and its applications on substrate-integrated waveguide filters," *IEEE Microw. Wireless Compon. Lett.*, Vol. 28, No. 11, 993–995, Nov. 2018.
9. Cameron, R. J., "Advanced coupling matrix synthesis techniques for microwave filters," *IEEE Trans. Microw. Theory Tech.*, Vol. 51, No. 1, 1–10, Jan. 2003.

10. He, Y., G. Macchiarella, G. Wang, W. Wu, L. Sun, L. Wang, and R. Zhang, "A direct matrix synthesis for in-line filters with transmission zeros generated by frequency-variant couplings," *IEEE Trans. Microw. Theory Tech.*, Vol. 66, No. 4, 1–10, Apr. 2018.
11. Li, G., "Coupling matrix optimization synthesis for filters with constant and frequency-variant couplings," *Progress In Electromagnetics Research Letters*, Vol. 82, 73–80, Mar. 2019.
12. Leszczynska, N., L. Szydlowski, and M. Mrozowski, "A novel synthesis technique for microwave bandpass filters with frequency-dependent couplings," *Progress In Electromagnetics Research*, Vol. 135, 35–50, 2013.
13. Su, Z. L., B. W. Xu, S. Y. Zheng, H. W. Liu, and Y. L. Long, "High-isolation and wide-stopband SIW diplexer using mixed electric and magnetic coupling," *IEEE Trans. Circuits Syst. II Express Briefs*, Vol. 67, No. 1, 32–36, Jan. 2019.
14. Cheng, F., X. T. Li, P. Lu, and K. Huang, "SIW filter with broadband stopband by suppressing the coupling of higher-order resonant modes," *Electron. Lett.*, Vol. 55, No. 25, 1345–1347, Dec. 2019.
15. Hong, J. S., *Microstrip Filters for RF/Microwave Applications*, A John Wiley & Sons, Inc., Hoboken, New Jersey, 2011.